JACS
JOURNAL OF THE AMERICAN CHEMICAL SOCIETY

Article

pubs.acs.org/JACS

Amine-Functionalized Lanthanide-Doped $KGdF_4$ Nanocrystals as Potential Optical/Magnetic Multimodal Bioprobes

Qiang Ju,[†] Datao Tu,[†] Yongsheng Liu,[†] Renfu Li,[†] Haomiao Zhu,[†,‡] Jincan Chen,[‡] Zhuo Chen,[‡] Mingdong Huang,[‡] and Xueyuan Chen*[,†,‡]

[†]Key Laboratory of Optoelectronic Materials Chemistry and Physics, Fujian Institute of Research on the Structure of Matter, Chinese Academy of Sciences, Fuzhou, Fujian 350002, China

[‡]State Key Laboratory of Structural Chemistry, Fujian Institute of Research on the Structure of Matter, Chinese Academy of Sciences, Fuzhou, Fujian 350002, China

Supporting Information

ABSTRACT: Amine-functionalized lanthanide-doped $KGdF_4$ nanocrystals, synthesized via a facile one-step solvothermal route by employing polyethylenimine as the surfactant and capping ligand, have been demonstrated to be sensitive time-resolved FRET bioprobes to detect a trace amount of biomolecules such as avidin at a concentration of 5.5 nM and to be potential T_1-MRI contrast agents due to a large longitudinal relaxivity of Gd^{3+} (5.86 $S^{-1}\cdot mM^{-1}$ per Gd ion and 3.99×10^5 $S^{-1}\cdot mM^{-1}$ per nanocrystal).

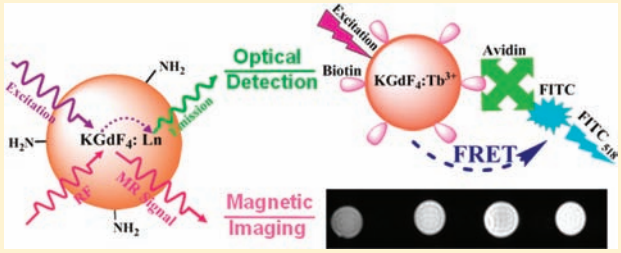

INTRODUCTION

Multifunctional and biocompatible nanoparticles (NPs), emerging as a new generation of multimodal bioprobes, have attracted reviving interest in a variety of bioapplications, offering potentials to overcome the current limitations of sensitivity and specificity in medical diagnoses and thus improve significantly the outcome of existing and emerging therapeutics.[1] Recently, optical/magnetic multimodal bioprobes have been fabricated by combining conventional luminescent materials such as organic dyes and semiconductor quantum dots (QDs) with superparamagnetic iron oxide NPs (e.g., Fe_3O_4, γ-Fe_2O_3), which can simultaneously provide a rapid detection of optical signals and a high spatial resolution of magnetic resonance imaging (MRI).[1a] However, these hybrid composites often confront the difficulties in integrating individual functions while preserving the original particle sizes. Besides, the toxicity of QDs, photobleaching of organic dyes, and negative (T_2) MRI contrast effect associated with iron oxide NPs further limit their practical applications to varying extents. As an alternative to these hybrid composites, trivalent lanthanide (Ln^{3+}) ion-doped Gd^{3+}-containing inorganic nanocrystals (NCs) have been proposed as a promising new class of multimodal bioprobes.[2] In comparison with organic dyes and QDs, Ln^{3+}-doped inorganic NCs show superior features, such as long luminescence lifetime (microsecond−millisecond range), large Stokes shift (>50 nm), narrow emission band widths (<10 nm), low toxicity, and high resistance to photobleaching, and thereby have been extensively applied in a variety of biodetection applications.[3] In particular, when combined with the technique of time-resolved (TR) luminescence that utilizes the long-lived emission of Ln^{3+} by setting appropriate delay time and gate time, the short-lived background luminescence or interferences such as scattered lights and autofluorescence from cells and tissues can be effectively suppressed, which thus results in high signal-to-noise ratio.[4] In contrast to iron oxide NPs, Gd^{3+} may induce the longitudinal relaxation of a water proton and has been well-established as the best known metal ion to serve as positive (T_1) MRI contrast agent so far.[5] Moreover, Gd^{3+}-containing inorganic NCs, which provide a more rigid crystal environment for Gd^{3+}, can more effectively lower the toxicity of free Gd^{3+} ion than clinically used chelated Gd^{3+} complexes and thus have been recognized as one of the most promising T_1-MRI contrast agents.[2a] On the other hand, owing to its distinct energy levels, Gd^{3+} can act as an efficient light-harvesting antenna (i.e., sensitizer) to absorb UV excitation light and subsequently transfer energy to activate its neighboring Ln^{3+}, giving rise to multicolor emissions of various Ln^{3+} ions (Figure 1).[6] To achieve intense photoluminescence (PL) of Ln^{3+}, inorganic fluoride NCs, particularly $AREF_4$ (A = alkali metal, RE = rare-earth) fluorides, such as $NaYF_4$ and $NaGdF_4$, have been most frequently employed as host materials for the doping of Ln^{3+} because of their high chemical stability and intrinsic low phonon energies (<350 cm^{-1}).[7] Recently, we have developed surface-functionalized GdF_3 and $NaYF_4$ NCs doped with Ln^{3+} as luminescent bioprobes to detect avidin through heterogeneous and homogeneous assays, respectively.[3e,f] $KGdF_4$ is another typical Gd^{3+}-containing host in the category of $AREF_4$; however, its optical and magnetic properties, as well as biocompatibility, have been rarely reported, not to mention its multimodal bioapplications.[8] In this work, amine-function-

Received: November 1, 2011
Published: December 6, 2011

   dx.doi.org/10.1021/ja2102604 | J. Am. Chem.Soc. 2012, 134, 1323−1330

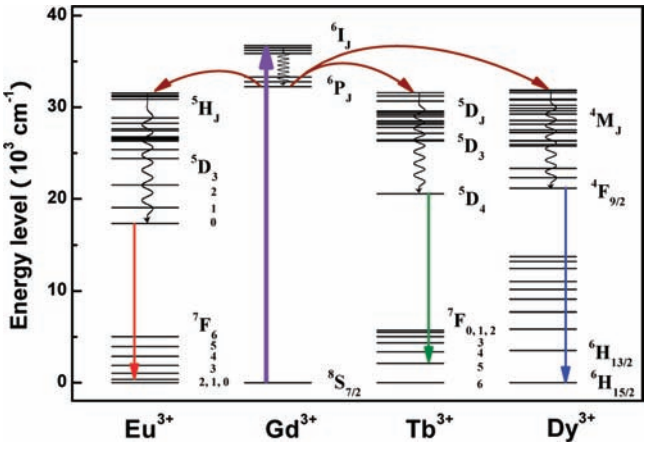

Figure 1. Schematic energy levels of Ln^{3+} ions describing the sensitized luminescence of Eu^{3+}, Tb^{3+}, and Dy^{3+} ions from Gd^{3+}. The curly arrows denote multiphonon nonradiative transitions, and the straight ones denote radiative transitions.

alized $KGdF_4$:Ln^{3+} (Ln = Eu, Tb, Dy) NCs, which can function as dual-mode (optical and magnetic) bioprobes, were synthesized through a facile one-pot solvothermal route. By employing the technique of time-resolved fluorescence resonance energy transfer (TR-FRET), we demonstrate for the first time the use of $KGdF_4$:Ln^{3+} NCs as luminescent bioprobes in a TR-FRET assay of avidin protein with a detection limit down to nanomolar range. The positive contrast enhancement induced by $KGdF_4$ NCs is also manifested in T_1 MRI experiments.

RESULTS AND DISCUSSION

Nanoparticle Characterization. Amine-functionalized Ln^{3+}-doped $KGdF_4$ NCs were synthesized through a facile one-step solvothermal method with polyethylenimine (PEI) as the surfactant and capping agent.[1g] PEI was selected to control the growth of NCs and further coated on the surface of NCs to provide a platform for direct linkage with biomolecules (Figure S1, Supporting Information). The ζ-potential for the NC colloidal solution was measured to be +23.2 mV (Figure S2, Supporting Information), indicative of positively charged PEI on the surface of NCs. Owing to the amino group capping on the surface, the $KGdF_4$ NCs can be steadily dispersed in water to form an optically transparent solution (Figure 2a). The as-prepared solution is very stable in air with no precipitate or aggregate observed after 1 month and remains stable under a variety of experimental conditions in terms of pH (from 3 to 12), temperature (from 0 to 45 °C), and salt concentration ($\lesssim$300 mM), suggesting that the $KGdF_4$:Ln^{3+} NC solution can withstand various biological conditions.[1f] TEM image shows that the as-prepared $KGdF_4$ NCs are roughly spherical with an average diameter of 25 ± 4 nm (Figure 2b,d). The corresponding high-resolution TEM (HRTEM) clearly demonstrates lattice fringes with an observed *d*-spacing of 0.34 nm (Figure 2c), which is in good agreement with the lattice spacing for the (111) plane of cubic $KGdF_4$ NCs.[8a] Powder XRD pattern of the NCs can be exclusively indexed to pure cubic phase of $KGdF_4$,[8a] indicating the presence of highly crystalline $KGdF_4$ NCs without any other impurities (Figure 2e). Composition analysis by energy-dispersive X-ray spectroscopy (EDS) reveals the presence of K, Gd, F, and doped Tb ions in $KGdF_4$:Tb^{3+} NCs (Figure 2f). It is worth mentioning that all

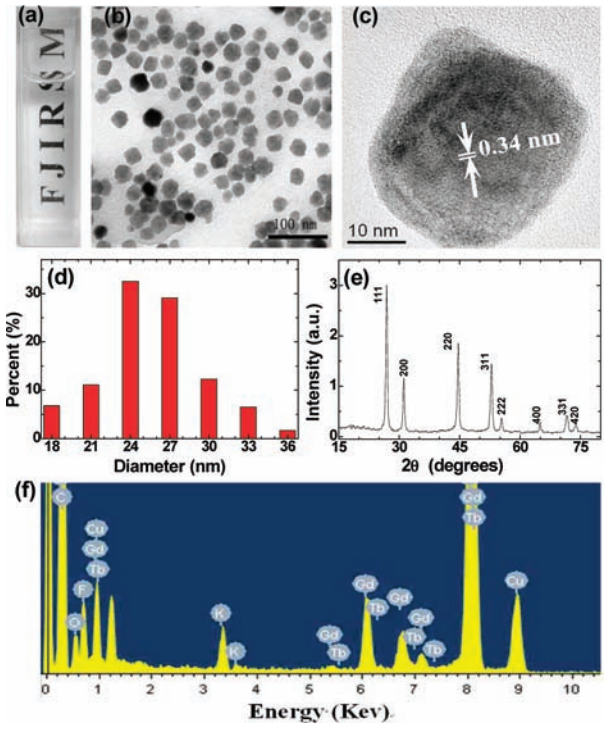

Figure 2. (a) Optically transparent solution of $KGdF_4$ NCs under daylight and (b) TEM, (c) HRTEM, (d) size distribution, (e) XRD pattern, and (f) EDS of monodispersed $KGdF_4$:Tb^{3+} NCs.

the NCs doped with different Ln^{3+} emitters exhibit essentially the same crystal phase and morphology.

Photoluminescence Properties. To demonstrate the performance and multicolor emissions of nanophosphors, PL excitation and emission spectra of $KGdF_4$ NCs doped with various Ln^{3+} emitters in aqueous solutions were measured at room temperature (RT). When the characteristic emissions of Eu^{3+}, Tb^{3+}, and Dy^{3+} at 593 ($^5D_0 \rightarrow {}^7F_1$), 545 ($^5D_4 \rightarrow {}^7F_5$), and 573 nm ($^4F_{9/2} \rightarrow {}^6H_{13/2}$), respectively, were monitored, all three excitation spectra (Figure 3a) were dominated by sharp excitation lines centered at 273 nm that correspond to the typical $^8S_{7/2} \rightarrow {}^6I_{7/2}$ transitions of Gd^{3+}, suggesting that the Ln^{3+} emissions can be realized through an energy transfer process from Gd^{3+} to Ln^{3+} dopants. In sharp contrast, much weaker excitation lines attributed to Eu^{3+}, Tb^{3+}, and Dy^{3+} ions were also observed, thus verifying that the Gd^{3+} sensitization is much more efficient than the direct excitation of the Ln^{3+} emitters. Upon excitation from the ground state $^8S_{7/2}$ to $^6I_{7/2}$ of Gd^{3+}, intense and distinct emission patterns of Eu^{3+}, Tb^{3+}, and Dy^{3+} were detected in the visible. These emission lines can be explicitly assigned to the transitions of $^5D_0 \rightarrow {}^7F_{0,1,2,3,4}$, $^5D_4 \rightarrow {}^7F_{6,5,4,3,2}$, and $^4F_{9/2} \rightarrow {}^6H_{15/2,13/2,11/2}$ for Eu^{3+}, Tb^{3+}, and Dy^{3+} and thus resulted in red, green, and blue color outputs without using any color filters, respectively (Figure 3a). The corresponding PL photographs of the NC solutions (1.0 mM) are shown in Figures 3c–e. The PL intensities of these NCs remain unchanged after UV irradiation for 12 h (radiation density of ~0.2 W/cm^2), indicative of the high photostability of NCs. According to cubic CaF_2 fluorite structure of $KGdF_4$, Ln^{3+} ions substituting for Gd^{3+} should possess a crystallographic O_h symmetry site randomly occupied by Gd^{3+} and K^+ cations.[3g] Theoretically, the $^5D_0 \rightarrow {}^7F_{0,2,4}$ emissions of electric-dipole nature should be strictly forbidden, and only the magnetic-dipole transition of $^5D_0 \rightarrow {}^7F_1$ would be allowed and thus be

dx.doi.org/10.1021/ja2102604 | J. Am. Chem.Soc. 2012, 134, 1323–1330

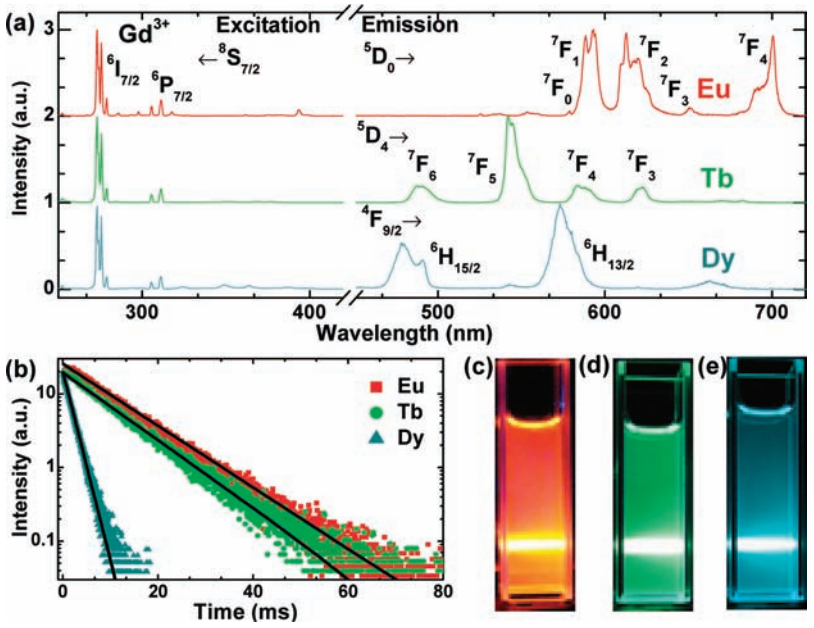

Figure 3. (a) RT excitation (left) and emission (right) spectra and (b) PL decay curves of Eu^{3+} (5.0 atom %), Tb^{3+} (5.0 atom %), and Dy^{3+} (0.5 atom %) singly doped $KGdF_4$ NCs in aqueous solutions (1.0 mM). Images c–e show PL photos from the corresponding solutions.

observed in the PL spectrum of Eu^{3+}.[3d] Interestingly, the integrated PL intensity of the $^5D_0 \rightarrow {}^7F_2$ transition peaked at 613 nm was found comparable to that of the $^5D_0 \rightarrow {}^7F_1$ transition peaked at 593 nm (Figure 3a). This also occurred to the $^5D_0 \rightarrow {}^7F_4$ transition centered at 699 nm. Most importantly, the appearance of the $^5D_0 \rightarrow {}^7F_0$ transition (~581 nm) in Figure 3a shows unambiguously that the site symmetry of Eu^{3+} in cubic $KGdF_4$ NCs should be restricted to C_s, C_n, or C_{nv} (n = 1, 2, 3, 4, 6).[3d] Similar phenomena were previously noticed but left unexplained in Er^{3+}- or Tm^{3+}-doped cubic (or hexagonal) $AREF_4$ NCs such as $NaYF_4$, $NaGdF_4$, and KYF_4, where the crystallographic site of O_h (or C_{3h}) is statistically occupied by two cations (A/RE).[3] This site symmetry descending from O_h may be induced by the substitution of Eu^{3+} for Gd^{3+} that slightly distorted the coordination structures such as bond distances around the O_h site originally statistically distributed by both Gd^{3+} and K^+.

To explore their potential applications in TR-FRET biodetection, we measured PL lifetimes of Eu^{3+} (5.0 atom %), Tb^{3+} (5.0 atom %), and Dy^{3+} (0.5 atom %) singly doped $KGdF_4$ NCs in aqueous solutions by monitoring their characteristic emissions at 593, 545, and 573 nm, respectively (Figure 3b). The decays from $^5D_0$ of Eu^{3+}, $^5D_4$ of Tb^{3+}, and $^4F_{9/2}$ of Dy^{3+} fit well to a single-exponential function, and their PL lifetimes were determined to be 10.34 ± 0.03, 9.48 ± 0.07, and 1.58 ± 0.01 ms for Eu^{3+}, Tb^{3+}, and Dy^{3+} singly doped NCs, respectively. Such single-exponential decay behavior usually indicates a homogeneous crystal-field environment around Ln^{3+} in the lattice sites. Table 1 compares the optical performance of some typical Tb^{3+}-based time-resolved luminescent bioprobes including commercially available Tb-DTPA-cs124 chelates. As shown in Table 1, $KGdF_4$:Tb^{3+} exhibits the largest Stokes shift with a value up to 272 nm, and the longest PL lifetime (9.48 ms) among those Tb^{3+}-based NCs and chelates. Owing to such a long PL lifetime in NCs, the luminescence of Ln^{3+} is expected to be distinguished easily from the undesired short-lived background fluorescence of organic dyes such as fluorescein isothiocyanate (FITC) by employing TR detection. FITC was

Table 1. Optical Properties of Typical Tb^{3+}-Based Time-Resolved Luminescent Bioprobes in Aqueous Solutions

	lifetime (ms)	Stokes shift (nm)	ref
Tb-DTPA-cs124	1.55	209	3i
Tb-DOTA-cs124	1.54	209	3i
Gd_2O_3:Tb	1.40	190	3k
LaF_3:Tb	3.20	57	3j
$NaYF_4$:Ce/Tb	4.76	252	3f
GdF_3:Tb	5.91	271	3e
$KGdF_4$:Tb	9.48	272	this work

intentionally chosen here as typical source of short-lived background fluorescence since its broadband emission partially overlaps with that of $KGdF_4$:Tb^{3+} NCs. The steady-state PL spectrum for the mixture of $KGdF_4$:Tb^{3+} (0.2 mM) and FITC (0.05 mM) was dominated by the emission of FITC (Figure 4a). Emission bands from Tb^{3+} were hardly observed due to the interference of the emission band from FITC and scattered lights. In sharp contrast, only intense emission lines originating from Tb^{3+} were detected in the TR spectrum (Figure 4b). These results confirm that the long-lived luminescence of Ln^{3+} coupled with the TR technique is very effective in removing undesired short-lived background fluorescence.

TR-FRET Detection of Avidin. The application of $KGdF_4$:Ln^{3+} NCs as sensitive TR-FRET bioprobes was further explored in an avidin–biotin model system.[4] The biotinylated NCs were prepared through the well-established EDC/NHS protocol (Figure S3, Supporting Information), in which biotin is covalently bound to amine-functionalized $KGdF_4$:Ln^{3+} NCs through its carboxylic group by using the cross-linking reagent 1-ethyl-3-(3-dimethyl aminopropyl) carboxylate (EDC) together with *N*-hydroxysuccinimide (NHS) in phosphate-buffered saline (PBS) solution.[1h] The successful attachment of biotin to the surface of NCs can be established through Fourier-transform infrared (FTIR) spectra and the specific recognition of FITC-labeled avidin for the NCs before and after bioconjugation (Figure 5a). For the PEI-capped NCs, weak

dx.doi.org/10.1021/ja2102604 | *J. Am. Chem.Soc.* 2012, 134, 1323–1330

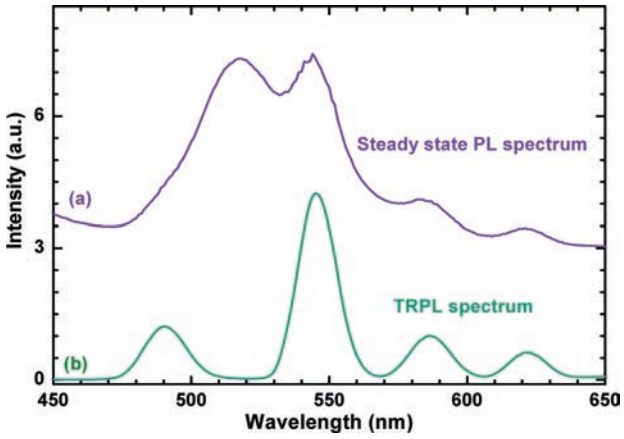

Figure 4. (a) Steady-state and (b) TR photoluminescence spectra (delay time = 200 μs, gate time = 3 ms) of the mixture of 0.2 mM $KGdF_4$:Tb^{3+} (5.0 atom %) NCs and 0.05 mM FITC, under excitation at 273 nm, demonstrate that the strong short-lived fluorescence of FITC detected in the steady-state mode can be completely suppressed under the TR detection mode.

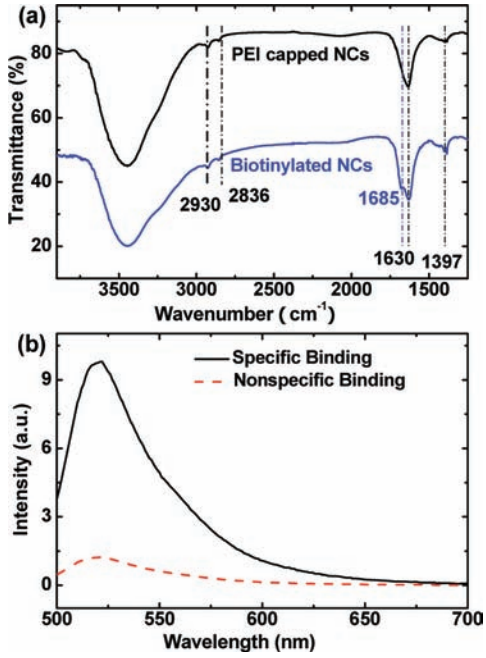

Figure 5. (a) FTIR spectra of biotinylated (upper line) and nonbiotinylated (bottom line) $KGdF_4$ NCs. (b) RT emission spectra of biotinylated (solid line) and nonbiotinylated (dashed line) $KGdF_4$ NCs after bioconjugation with FITC-labeled avidin.

IR peaks at 1397, 2930, and 2836 cm^{-1} are attributed to the stretching vibrations of the C−N bond and asymmetric and symmetric stretching vibrations of the C−H bond, respectively; a strong IR band centered at 1630 cm^{-1} was observed, which can be attributed to the N−H bending mode of amino group (−NH_2), thereby revealing the PEI capping on the surface of NCs. After biotinylation, a new distinguishable IR band at 1685 cm^{-1} was observed for the biotinylated NCs, which is ascribed to the stretching vibration of the amide bond. This feature verifies the successful binding of $KGdF_4$ NCs with biotin. The selective recognition of NCs for FITC-labeled avidin was witnessed by monitoring the PL intensity from FITC.[2b] Upon incubation with the FITC-labeled avidin, the biotinylated NCs showed remarkable increase in the PL signal of FITC relative to the nonbiotinylated NC counterparts (Figure 5b). Homogeneous-type FRET assay, which makes use of distance-dependent energy transfer between an excited donor fluorophore and an acceptor fluorophore through long-range dipole−dipole interactions to detect the target biomolecules and thus free from the laborious separation and centrifugation typical in heterogeneous assays,[1j] was introduced for the detection of trace amount of avidin protein in the solution. In a typical FRET, excitation of the donor by an energy source (e.g., flash lamp or laser) triggers an energy transfer to the acceptor provided that they are within a given proximity to each other and spectrally overlapped between the absorption of acceptor and the emission of donor, and the acceptor in turn emits light at its given wavelength.[4] FITC and $KGdF_4$:Tb^{3+} NCs were selected as acceptor and donor labels, respectively, in the avidin−biotin system. The absorption spectrum of FITC matches well with the emission band of Tb^{3+} at 488 nm (hereafter referred to as Tb_{488}), and the emission band of FITC centered at ∼518 nm (hereafter referred to as $FITC_{518}$) is located between the two emission bands (488 and 545 nm) of Tb^{3+} (Figure S4, Supporting Information). To avoid the interference of the short-lived background fluorescence from directly excited FITC, we employed the TR technique utilizing the long-lived luminescence of Ln^{3+} in the FRET measurements.[4] The combination of FRET and TR techniques brings together the benefit of extremely low background from TR detection and the convenience of homogeneous assay from FRET.

The process for a homogeneous TR-FRET assay (Figure 6a) is as follows: after adding the same volume of biotinylated $KGdF_4$:Tb^{3+} NC solution to microplate wells, different amounts of avidin labeled with FITC were added and incubated for 0.5 h at RT, during which the biotinylated NCs were conjugated with avidin via a sensitive and specific interaction between avidin and biotin. The microplate was subjected to TR-FRET measurements on a Synergy 4 microplate reader (BioTeK). The concentration of avidin can be quantified by measuring the integrated PL intensity ratio of $FITC_{518}/Tb_{488}$, a figure of merit derived from the deconvolution of the TR-FRET spectrum (Figure S5, Supporting Information) to characterize the efficiency of energy transfer from Tb^{3+} to FITC. As shown in Figure 6b, the TR-FRET signal represented by $FITC_{518}$ was gradually enhanced at the expense of Tb_{488} with increasing amount of FITC-labeled avidin, thus quantitatively visualizing the binding and FRET between FITC-labeled avidin and biotinylated NCs. For comparison, nonbinding control experiments were performed by employing the as-prepared NCs instead of the biotinylated NCs as bioprobes under otherwise identical conditions. The calibration curve (Figure 6c) demonstrates that the TR-FRET signal of $FITC_{518}/Tb_{488}$ gradually increases with the avidin concentration ranging from 4.5 to 1800 nM and tends to saturate at higher concentration than 600 nM. Nonbiotinylated NCs and FITC were far apart in the solution, and thus no FRET occurred in the control experiments (Figure S6, Supporting Information). As a result, the TR-FRET signals observed in the control experiments remain very low for the avidin concentration from 4.5 to 1800 nM. The detection limit, defined as the concentration that corresponds to three times the standard deviation above the signal measured in the control experiment, is 5.5 nM. The detection limit based on TR-FRET bioprobes that we developed is comparable to previous results

dx.doi.org/10.1021/ja2102604 | J. Am. Chem.Soc. 2012, 134, 1323−1330

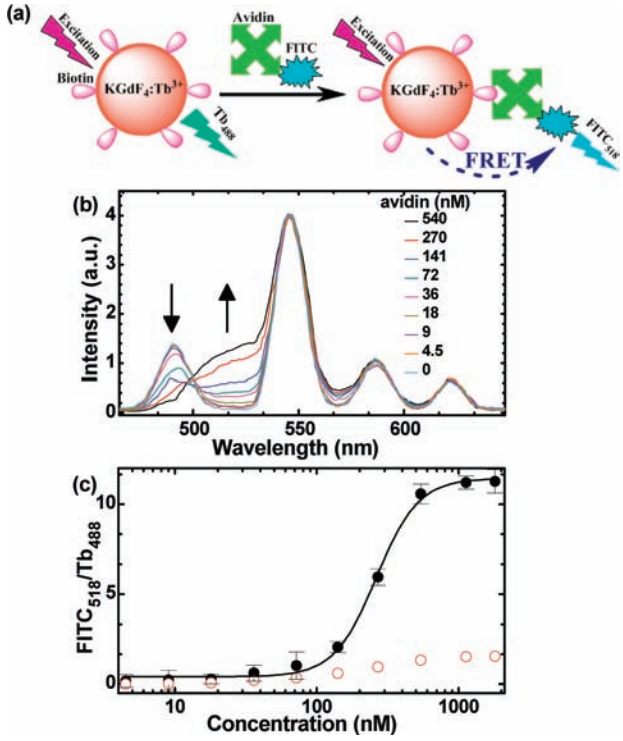

Figure 6. (a) Schematic illustration of the TR-FRET detection of avidin. (b) TR-FRET spectra of the bioassays at different concentrations of avidin as indicated (nM). The spectra were normalized to unity at the maximum emission peak at 545 nm, and each data point represents average of quintuplicate measurements. (c) Calibration curve of the TR-FRET detection by employing biotinylated $KGdF_4:Tb^{3+}$ NCs as bioprobes for the detection of avidin (the *X*-axis is in log scale). The filled symbols show bioassay experiments where FITC is FRET-sensitized by NCs through the avidin–biotin interaction. The open symbols show the control experiments employing nonbiotinylated NC counterparts.

based on the steady-state competitive FRET (or upconversion FRET) assay that utilized QDs (or $NaYF_4$:Er/Yb NCs) as donor and Au NPs as nonluminescent quencher to detect avidin with a detection limit of 0.5–10 nM.[1j,3c]

***T_1* Magnetic Resonance Imaging.** To evaluate the potential application of amine-functionalized $KGdF_4$ NCs as T_1-MRI contrast agent, we measured the magnetic field dependency of the NCs (Figure 7a). The magnetization curve of $KGdF_4$ NCs shows typical paramagnetic behavior, as commonly observed for T_1-MRI contrast agents. The mass magnetic susceptibility of $KGdF_4$ NCs was determined to be $(9.85 \pm 0.01) \times 10^{-5}$ emu·Oe^{-1}·g^{-1} (namely, $(7.84 \pm 0.01) \times 10^{-3}$ m^3·kg^{-1}) from the magnetization slope, and the RT magnetization is 1.97 emu·g^{-1} (1.97 A·m^2·kg^{-1}) at 20 KOe, which approximates the reported value (3.2 emu·g^{-1}) of Fe_3O_4 NPs used for magnetic bioseparation.[2d] The longitudinal relaxation time (T_1) was measured in aqueous solutions with different Gd^{3+} concentrations. From the slope of the plot of $1/T_1$ versus the Gd^{3+} concentration (Figure 7b), the ionic longitudinal relaxivity (r_1) was determined to be 5.86 ± 0.18 S^{-1}·mM^{-1}. Table 2 compares the ionic longitudinal relaxivity of some typical MRI contrast agents. As shown in Table 2, $KGdF_4$ that we developed shows much larger longitudinal relaxivity per Gd ion than most Gd^{3+}-based inorganic NCs recently reported, and molecular probes such as Gd-DTPA chelate, a widely used clinical MRI contrast agent, under identical measurement

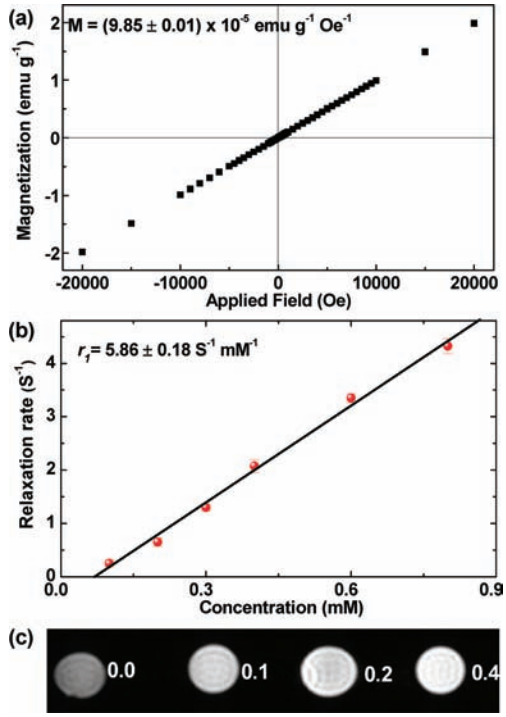

Figure 7. (a) RT magnetization as a function of magnetic field for $KGdF_4$ NCs. (b) ^1H spin–lattice relaxation rates ($1/T_1$) of H_2O as a function of molar concentration (mM) of $KGdF_4$ NCs in a 80/20 (v/v) H_2O/D_2O mixture at RT and 9.4 T. (c) T_1-weighted MRI of $KGdF_4$ NCs at various concentration in water (mM).

Table 2. Ionic Longitudinal Relaxivity of Typical MRI Contrast Agents

	size (nm)	r_1 (S^{-1} mM^{-1})	ref
Gd-DTPA		5.30	9
Gd-DOTA		4.10	2e
GdF_3	30–50	1.44	3e
$GdPO_4$	50–90	1.60	2f
Gd_2O_3	4–8	4.40	2e
$NaGdF_4$	20–25	6.18	7d
$NaGdF_4$	2–3	7.2	7e
$KGdF_4$	18–36	5.86	this work

condition. The remarkable enhancement of r_1 may be attributed to the small particle size of the $KGdF_4$ NC (~25 nm) with high surface-to-volume ratio, which renders more Gd^{3+} ions residing on the surface and thus significantly contributes to the longitudinal relaxation of the water proton.[7b] Moreover, since a single NC contains many Gd^{3+} ions (more than 10^4 per NC), $KGdF_4$ NCs are expected to provide much higher signal than a single-molecule-based probe. To quantitatively estimate the longitudinal relaxivity per $KGdF_4$ NC, we assume that only Gd ions residing within a spherical shell (<5 nm) of each $KGdF_4$ NC (diameter of 25 nm) contribute to the observed relaxivity, based on the fact that the close-to-surface Gd^{3+} ions in NCs play a dominant role in changing the relaxation of the water proton. The longitudinal relaxivity per $KGdF_4$ NC was calculated to be 3.99×10^5 S^{-1}·mM^{-1}, which is 7.5×10^4 times larger than that of Gd-DTPA (Figure S7, Supporting Information). It should be noted that although the 2.5 nm $NaGdF_4$ in Table 2 exhibits a larger ionic longitudinal relaxivity than that of our work, the longitudinal relaxivity per $NaGdF_4$ NC (770 S^{-1}·mM^{-1})

dx.doi.org/10.1021/ja2102604 | J. Am. Chem.Soc. 2012, 134, 1323–1330

reported by van Veggel is approximately 0.2% of ours because it contains much fewer Gd^{3+} ions.[7e] In the proof-of-concept application as T_1 MRI contrast agents (Figure 7c), representative T_1-weighted magnetic resonance images of the NC suspensions clearly showed the positive enhancement effect on T_1-weighted sequences as the NC concentration increases, indicating that $KGdF_4$ NCs may serve as an effective T_1 MRI contrast agent.

Cytotoxicity. For bioimaging and biodetection, it is critically important to evaluate the toxicity of NC-based bioprobes. Herein, the NC effect on cell proliferation was estimated with human embryo lung fibroblasts (HELF) cells. The HELF cells were first grown with the medium containing different concentrations of $KGdF_4$ NCs (0−800 μg mL^{-1}) for 24 h, and then the cell viability was determined on the basis of Cell Counting Kit-8 (CCK-8) assay. Upon incubation with NCs (200 μg mL^{-1}), only less than 6% of the HELF cells died (Figure 8). Even at higher concentrations (800 μg mL^{-1}) of

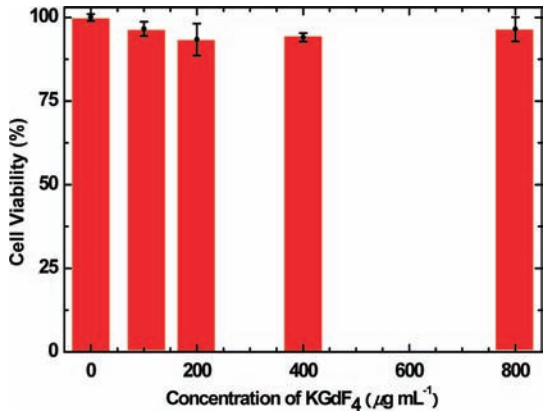

Figure 8. In vitro cytotoxicity of $KGdF_4$ NCs against HELF cell after 24 h incubation.

$KGdF_4$ NCs, the cell viability still remained above 95%. On the basis of these CCK-8 assay results, it can be inferred that amine-functionalized $KGdF_4$:Ln^{3+} NCs are biocompatible and nearly nontoxic to live cells. Their low cytotoxicity implies that $KGdF_4$:Ln^{3+} can serve as safe luminescent biolabels and MRI contrast agents.

CONCLUSIONS

We have synthesized amine-functionalized and biocompatible $KGdF_4$:Ln^{3+} NCs through a facile one-step solvothermal route by employing PEI as capping ligand. The resultant NCs can be readily conjugated to biomolecules through amino groups on the surface of NCs and further serve as functional bioprobes. By varying the doped Ln^{3+} emitters, we have achieved intense long-lived multicolor emissions under single-wavelength excitation in $KGdF_4$:Ln^{3+} NCs. Spectroscopic evidence reveals the distorted site symmetry of Ln^{3+} around the crystallographic O_h site originally occupied statistically by both Gd^{3+} and K^+. The surface-functionalized $KGdF_4$:Tb^{3+} NCs have been demonstrated as a sensitive bioprobe in TR-FRET assays to quantitatively detect avidin protein with a detection limit down to 5.5 nM. Furthermore, the $KGdF_4$ NCs possess a relatively large longitudinal relaxivity (5.86 S^{-1}·mM^{-1} per Gd ion and 3.99 × 10^5 S^{-1}·mM^{-1} per NC) among fluoride NCs previously reported, and the molar relaxivity per $KGdF_4$ NC is approximately estimated to be 4 orders of magnitude larger than that of commercial Gd-DTPA. As an alternative to traditional organic fluorophores, lanthanide chelates or QDs, amine-functionalized $KGdF_4$:Ln^{3+} NCs feature superior optical properties (long-lived PL and multicolor tuning) and positive T_1 MRI contrast effect and thus are highly promising for versatile bioapplications such as time-resolved biodetection, DNA hybridization, magnetic bioseparation, and multimodal bioimaging.

EXPERIMENTAL DETAILS

Chemicals and Materials. Ethylene glycol, ethanol, methanol, and 2,5-dimethylformamide (DMF) were purchased from Sinopharm Chemical Reagent Co., China. Fluorescein isothiocyanate (FITC), 1-ethyl-3-(3-dimethyl aminopropyl) carboxylate (EDC), *N*-hydroxysuccinimide (NHS), avidin, and biotin were purchased from Sigma-Aldrich Co. Polyethylenimine aqueous solution (30% in V/V, PEI) was purchased from TCI (Shanghai) Development Co., Ltd. Human embryo lung fibroblasts (HELF) cells and Cell Counting Kit-8 were purchased from Shanghai Institute of Cell Biology, Chinese Academy of Sciences, and Beyotime Institute of Biotechnology, China, respectively. The opaque microtitration microplate (Costar 3641) was purchased from Corning Inc.

Synthesis of $KGdF_4$:Ln^{3+} NCs. Typically, a well-stirred transparent solution of 30 mL of ethylene glycol with 1.0 mmol KCl, 0.05 mmol $EuCl_3$·$6H_2O$ (or 0.05 mmol $TbCl_3$·$6H_2O$ or 0.005 mmol $DyCl_3$·$6H_2O$), required amount of $GdCl_3$·$6H_2O$, and 1 mL of PEI aqueous solution were added with a stoichiometric amount of NH_4F in 10 mL of ethylene glycol. The mixture was stirred for another 20 min, transferred into a 50 mL Teflon-lined autoclave, and subsequently heated at 200 °C for 4 h. After cooling to room temperature (RT), the obtained NCs were collected by centrifugation, washed with ethanol and water several times, and dried in vacuum at 60 °C for 10 h.

Cytotoxicity of $KGdF_4$ NCs. HELF cells were routinely maintained in RPMI-1640 medium (GIBCO BRL) supplemented with 10% (v/v) heat-inactivated fetal calf serum (FCS), penicillin (100 U mL^{-1}), and streptomycin (100 U mL^{-1}). Cells were seeded into a 96-well culture plate at 2 × 10^4 cells/well and cultured at 37 °C under humidified air containing 5% CO_2 for 24 h before a series of concentrations of $KGdF_4$ NC (0, 100, 200, 400, and 800 μg/mL in RPMI 1640) were added. Cells were then incubated at 37 °C under 5% CO_2 for another 24 h. Cell Counting Kit-8 was subsequently applied to the cells followed by incubation at 37 °C under 5% CO_2 for 4 h. The OD_{450} value of each well was measured on a Synergy 4 hybrid multimode microplate reader (BioTek). The following formula was applied to calculate the inhibition rate of cell growth: cell viability (%) = ({mean of absorbance value of treatment group}/{mean of absorbance value of control}) × 100%.

Synthesis of Biotinylated $KGdF_4$:Ln^{3+} NCs. The conjugation of $KGdF_4$:Ln^{3+} NCs with biotin was achieved by utilizing a cross-linking reagent, EDC. This compound reacts with the surface carboxyl (−COOH) group on the biotin to yield an *O*-acylisourea active intermediate (Figure S3, Supporting Information), which is then attacked by a primary amine (NH_2) group on the NCs to form a stable covalent bond between the biotin and the $KGdF_4$ NCs. One drawback to this procedure is that the intermediate formed in the EDC reaction is subject to hydrolysis in aqueous media. To increase the reaction yield, a second reagent, NHS, was added to form a more stable active ester intermediate. This intermediate is less susceptible to hydrolysis, while at the same time reacts more rapidly with amines. In a typical procedure, 64 mg of biotin, 90 mg of NHS, and 110 mg of EDC were added to 20 mL of phosphate-buffered saline (PBS) solution (pH = 7.2) and stirred for 2 h. Then, 20 mg of $KGdF_4$:Ln^{3+} NCs was added, and the mixture was stirred slowly for 20 h at RT. The excess biotin, EDC, and NHS were removed by three cycles of centrifugation separation, washing, and redispersion. The biotinylated NCs were dispersed in 10 mL of water and stored at 4 °C.

Synthesis of FITC-Labeled Avidin. The avidin labeled with FITC was synthesized through a reported procedure.[1h] Avidin (30 mg) was dissolved in 10 mL of 0.1 M sodium carbonate buffer (pH = 9.5).

Meanwhile, 5 mg of FITC was dissolved in 10 mL of 2,5-dimethylformamide (DMF), which should be protected from light. Then 0.1 mL of FITC solution was added to 1 mL of avidin solution and reacted overnight at 4 °C in the dark. The excess FITC was removed via extensive dialysis for 48 h using a membrane of molecular weight cutoff of 10 000 Da. FITC quantification was performed by detection with UV absorption of the solution at λ = 494 nm. The extinction coefficient at this wavelength for FITC is 70 000 M^{-1} cm^{-1}. The number of FITC per avidin molecule was approximately determined to be 3.6.

Conjugation of Biotinylated $KGdF_4$ NCs with FITC-Labeled Avidin. Biotinylated $KGdF_4$ NCs (5 mg) were suspended in 5 mL of 0.1 M PBS solution (pH = 7.2), followed by the addition of FITC-labeled avidin (0.2 mL) and incubation for 0.5 h at RT. The NCs were then isolated by centrifugation, washed several times with PBS solution, and resuspended in PBS solution (2 mL).

Characterization. Powder X-ray diffraction (XRD) patterns were collected using a RIGAKU DMAX2500PC powder diffractometer with Cu Kα_1 radiation (λ = 0.154 nm). Both the low- and high-resolution TEM measurements were performed using a JEOL-2010 TEM equipped with the energy-dispersive X-ray spectrum (EDS). The infrared spectra were recorded on a Magna 750 Fourier-transform infrared spectrometer (FTIR). The ζ-potential of the NC solution was determined by using a dynamic light scattering (DLS) instrument (ZETASIZER 3000, Malvern Instruments Ltd.). Emission and excitation spectra and transient decays were recorded on an Edinburgh Instruments FLS920 spectrofluorimeter equipped with both continuous (450 W) and pulsed xenon lamps at RT. PL photographs of the NC solution were taken with Nikon digital single lens reflex D100 upon excitation by the third-harmonic generation (THG) of a mode-locked picosecond Ti:sapphire laser (1 mW@273 nm, Tsunami, Spectra-Physics). The time-resolved photoluminescence (TR-PL) spectra in this work were carried out on a Synergy 4 multimode microplate reader with hybrid technology (BioTek). The magnetic properties of $KGdF_4$ NCs were measured on a superconducting quantum interference device (SQUID) magnetometer (MPMS-7, Quantum Design) at RT.

Homogeneous TR-FRET Detection of Avidin by Employing Biotinylated $KGdF_4$:Tb^{3+} NCs. Biotinylated $KGdF_4$:Tb^{3+} solution (100 μL, 0.5 μg/mL) was added to the wells of a 96-well microplate, and then 100 μL of FITC-labeled avidin with different concentrations were added. After incubation for 30 min at RT, the plate was subjected to TR-PL detection on a BioTeK Synergy 4 multimode microplate reader at RT. The excitation wavelength was 273 nm, and the delay time and gate time were set to be 200 μs and 3 ms, respectively.

Relaxivity Measurement of $KGdF_4$:Ln^{3+} NCs as Magnetic Resonance Imaging Contrast Agents. The solvent longitudinal relaxation times (T_1) for $KGdF_4$ NCs dispersed in aqueous solution (H_2O/D_2O = 80/20) were measured by a standard inversion–recovery pulse sequence on a Bruker Avance III NMR spectrometer at 20 °C and 9.4 T (400 MHz). The ability of proton relaxation enhancement of $KGdF_4$ NC is expressed by the term ionic relaxivity r_1, which is defined as the slope of the following equation[9] in the units of mM^{-1} S^{-1}:

$$(1/T_1)_{obs} = (1/T_1)_d + r_1[M]$$

where $(1/T_1)_{obs}$ and $(1/T_1)_d$ are the observed values in the presence and absence of the paramagnetic species ($KGdF_4$) and [M] is the concentration of the paramagnetic species ($KGdF_4$).

The T_1-weighted magnetic resonance images were acquired at RT using a 3 T Biospec Bruker Advance MR scanner (GmbH, Ettlingen, Germany). Dilutions of $KGdF_4$ NCs (0, 0.1, 0.2, 0.4 mM) in water were placed in a series of 1 mL tubes for T_1-weighted MRI. The following parameters were adopted: repetition time (TR) = 50 ms, echo time (TE) = 3 ms, matrix size =128 pixels ×128 pixels, field of view (FOV) = 90, and slice thickness = 1 mm.

■ ASSOCIATED CONTENT

Supporting Information

Schematic illustration and ζ-potential of PEI-capped $KGdF_4$ NCs, biotinylation of NCs, PL spectra of $KGdF_4$:Tb^{3+} NCs and FITC, PL spectra of TR-FRET detection, and calculation of longitudinal relaxivity per $KGdF_4$ NC. This material is available free of charge via the Internet at http://pubs.acs.org.

■ AUTHOR INFORMATION

Corresponding Author

xchen@fjirsm.ac.cn

■ ACKNOWLEDGMENTS

This work is supported by the Hundred Talent Program of the Chinese Academy of Sciences (CAS), Knowledge Innovation Program of CAS for Key Topics (Grant No. KJCX2-YW-358), the NSFC (Grant Nos. 10974200, 51002151 and 51102234), the 863 programs of MOST (Grant Nos. 2009AA03Z430, and 2011AA03A407), and the NSF of Fujian Province for Young Scientists (Grant No. 2010J05126).

■ REFERENCES

(1) (a) Louie, A. *Chem. Rev.* **2010**, *110*, 3146. (b) Wang, J.; Tanner, P. A. *J. Am. Chem. Soc.* **2010**, *132*, 947. (c) Haase, M.; Schäfer, H. *Angew. Chem., Int. Ed.* **2011**, *50*, 5808. (d) Li, C. X.; Lin, J. *J. Mater. Chem.* **2010**, *20*, 6831. (e) Murray, C. B.; Ko, D. K. *ACS Nano* **2011**, *5*, 4810. (f) Huh, Y. M.; Jun, Y. W.; Song, H. T.; Kim, S.; Choi, J. S.; Lee, J. H.; Yoon, S.; Kim, K. S.; Shin, J. S.; Suh, J. S.; Cheon, J. *J. Am. Chem. Soc.* **2005**, *127*, 12387. (g) Wang, F.; Liu, X. G. *J. Am. Chem. Soc.* **2008**, *130*, 5642. (h) Hermanson, G. T. *Bioconjugate Techniques*; Academic Press: New York, 1996. (i) Lin, C. C.; Xiao, Z. R.; Guo, G. Y.; Chan, T. S.; Liu, R. S. *J. Am. Chem. Soc.* **2010**, *132*, 3020. (j) Wang, L. Y.; Yan, R. X.; Hao, Z. Y.; Wang, L.; Zeng, J. H.; Bao, H.; Wang, X.; Peng, Q.; Li, Y. D. *Angew. Chem., Int. Ed.* **2005**, *44*, 6054. (k) Bogdan, N.; Vetrone, F.; Ozin, G. A.; Capobianco, J. A. *Nano Lett.* **2011**, *11*, 835. (l) Vetrone, F.; Naccache, R.; Zamarron, A.; de la Fuente, A. J.; Sanz-Rodriguez, F.; Maestro, L. M.; Rodriguez, E. M.; Jaque, D.; Sole, J. G.; Capobianco, J. A. *ACS Nano* **2010**, *4*, 3254. (m) Zhang, Y. W.; Mai, H. X.; Si, R.; Yan, Z. G.; Sun, L. D.; You, L. P.; Yan, C. H. *J. Am. Chem. Soc.* **2006**, *128*, 6426. (n) Deng, R. R.; Xie, X. J.; Vendrell, M.; Chang, Y.-T.; Liu, X. G. *J. Am. Chem. Soc.* **2011**, *133*, 20168.

(2) (a) Na, H. B.; Song, I. C.; Hyeon, T. *Adv. Mater.* **2009**, *21*, 2133. (b) Wang, F.; Liu, X. G. *Chem. Soc. Rev.* **2009**, *38*, 976. (c) Kumar, R.; Nyk, M.; Ohulchanskyy, T. Y.; Flask, C. A.; Prasad, P. N. *Adv. Funct. Mater.* **2009**, *19*, 853. (d) Wong, H. T.; Chan, H. L. W.; Hao, J. H. *Appl. Phys. Lett.* **2009**, *95*, No. 122512. (e) Bridot, J. L.; Faure, A. C.; Laurent, S.; Rivière, C.; Billotey, C.; Hiba, B.; Janier, M.; Josserand, V.; Coll, J. L.; Vander Elst, L.; Muller, R.; Roux, S.; Perriat, P.; Tillement, O. *J. Am. Chem. Soc.* **2007**, *129*, 5076. (f) Yoon, Y.-s.; Lee, B.-II.; Lee, K. S.; Heo, H.; Lee, J. H.; Byeon, S.-H.; Lee, I. S. *Chem. Commun.* **2010**, *46*, 3654.

(3) (a) Karsten, K.; Holger, B.; Jog, S.; Arun, L.; Sorin, A.; Thomas, M.; Markus, H. *Angew. Chem., Int. Ed.* **2003**, *42*, 5513. (b) Li, Z. Q.; Zhang, Y.; Jiang, S. *Adv. Mater.* **2008**, *20*, 4765. (c) Oh, E.; Hong, M. Y.; Lee, D.; Nam, S. H.; Yoon, H. C.; Kim, H. S. *J. Am. Chem. Soc.* **2005**, *127*, 3270. (d) Ju, Q.; Liu, Y. S.; Li, R. F.; Liu, L. Q.; Luo, W. Q.; Chen, X. Y. *J. Phys. Chem. C* **2009**, *113*, 2309. (e) Ju, Q.; Liu, Y. S.; Tu, D. T.; Zhu, H. M.; Li, R. F.; Chen, X. Y. *Chem.—Eur. J.* **2011**, *17*, 8549. (f) Tu, D. T.; Liu, L. Q.; Ju, Q.; Liu, Y. S.; Zhu, H. M.; Li, R. F.; Chen, X. Y. *Angew. Chem., Int. Ed.* **2011**, *50*, 6306. (g) Yang, D.; Li, C.; Li, G.; Shang, M.; Kang, X.; Lin, J. *J. Mater. Chem.* **2011**, *21*, 5923. (h) Wang, Z. L.; Quan, Z. W.; Jia, P. Y.; Lin, C. K.; Luo, Y.; Chen, Y.; Fang, J.; Zhou, W.; O'Connor, C. J.; Lin, J. *Chem. Mater.* **2006**, *18*, 2030. (i) Li, M.; Selvin, P. R. *J. Am. Chem. Soc.* **1995**, *117*, 8132. (j) Sivakumar, S.; Diamente, P. R.; van Veggel, F. C. *Chem.—Eur. J.* **2006**, *12*, 5878. (k) Louis, C.; Bazzi, R.; Marquette, C. A.; Bridot, J. L.;

Roux, S.; Ledoux, G.; Mercier, B.; Blum, L.; Perriat, P.; Tillement, O. *Chem. Mater.* **2005**, *17*, 1673.
(4) (a) Bunzli, J. C. G. *Chem. Rev.* **2010**, *110*, 2729. (b) Morgner, F.; Geißler, D.; Stufler, S.; Butlin, N. G.; Lohmannsroben, H. G.; Hildebrandt, N. *Angew. Chem., Int. Ed.* **2010**, *49*, 7570.
(5) (a) Evanics, F.; Diamente, P. R.; van Veggel, F. C. J. M.; Stanisz, G. J.; Prosser, R. S. *Chem. Mater.* **2006**, *18*, 2499. (b) Hifumi, H.; Yamaoka, S.; Tanimoto, A.; Citterio, D.; Suzuki, K. *J. Am. Chem. Soc.* **2006**, *128*, 15090. (c) Zhou, J.; Sun, Y.; Du, X. X.; Xiong, L. Q.; Hu, H.; Li, F. Y. *Biomaterials* **2010**, *31*, 3287.
(6) (a) Liu, Y. S.; Tu, D. T.; Zhu, H. M.; Li, R. F.; Luo, W. Q.; Chen, X. Y. *Adv. Mater.* **2010**, *22*, 3266. (b) Lorbeer, C.; Cybinska, J.; Mudring, A. V. *Chem. Commun.* **2010**, *46*, 571. (c) Yang, D.; Kang, X.; Shang, M.; Li, G.; Peng, C.; Li, C.; Lin, J. *Nanoscale* **2011**, *3*, 2589. (d) Li, C.; Ma, P.; Yang, P.; Xu, Z.; Li, G.; Yang, D.; Peng, C.; Lin, J. *CrystEngComm* **2011**, *13*, 1003.
(7) (a) Ptacek, P.; Schäfer, H.; Kömpe, K.; Haase, M. *Adv. Funct. Mater.* **2007**, *17*, 3843. (b) Chen, G. Y.; Ohulchanskyy, T. Y.; Kumar, R.; Agren, H.; Prasad, P. N. *ACS Nano* **2010**, *4*, 3163. (c) Wang, F.; Deng, R. R.; Wang, J.; Wang, Q. X.; Han, Y.; Zhu, H. M.; Chen, X. Y.; Liu, X. G. *Nat. Mater.* **2011**, *10*, 968. (d) Chen, F.; Bu, W.; Zhang, S.; Liu, X.; Liu, J.; Xing, H.; Xiao, Q.; Zhou, L.; Peng, W.; Wang, L.; Shi, J. *Adv. Funct. Mater.* **2011**, *21*, 4285. (e) Johnson, N. J. J.; Oakden, W.; Stanisz, G. J.; Scott Prosser, R.; van Veggel, F. C. J. M. *Chem. Mater.* **2011**, *23*, 3714.
(8) (a) Du, Y. P.; Zhang, Y. W.; Sun, L. D.; Yan, C. H. *Dalton. Trans.* **2009**, 8574. (b) Schäfer, H.; Ptacek, P.; Zerzouf, O.; Haase, M. *Adv. Funct. Mater.* **2008**, *18*, 2913. (c) Wong, H.-T.; Vetrone, F.; Naccache, R.; Chan, H. L. W.; Hao, J.; Capobianco, J. A. *J. Mater. Chem.* **2011**, *21*, 16589. (d) Yang, L. W.; Zhang, Y. Y.; Li, J. J.; Li, Y.; Zhong, J. X.; Chu, P. K. *Nanoscale* **2010**, *2*, 2805.
(9) Li, W. S.; Li, Z. F.; Jing, F. Y.; Deng, Y. F.; Wei, L.; Liao, P.; Yang, X. G.; Li, X. J.; Pei, F. K.; Wang, X. X.; Lei, H. *Carbohydr. Res.* **2008**, *343*, 685.